X-ray diffraction study of Mn/Sb multilayered films with artificial superstructures

1990 J. Phys.: Condens. Matter 2 9717

(http://iopscience.iop.org/0953-8984/2/49/001)

J. Phys.: Condens. Matter **2** (1990) 9717–9733. Printed in the UK

X-ray diffraction study of Mn/Sb multilayered films with artificial superstructures

I Moritani, N Nakayama and T Shinjo
Institute for Chemical Research, Kyoto University, Uji 611, Japan

Received 27 February 1990, in final form 2 July 1990

Abstract. Structures of Mn/Sb multilayered films have been investigated by x-ray diffraction. MnSb/Sb superlattice films are obtained when the nominal thicknesses are [Mn(1 Å)/Sb(50 Å)]$_{90}$ and [Mn(2 Å)/Sb(50 Å)]$_{90}$. Ultrathin layers of MnSb are formed by interfacial reaction in these samples with keeping an epitaxial orientation of $(00.1)_{MnSb}\|(00.1)_{Sb}$; $[11.0]_{MnSb}\|[11.0]_{Sb}$. These films have fibre texture structures with an in-plane coherence length of about 300 Å. The distribution of growth orientation is approximated by a Gaussian distribution function with a half-width of about 10°. The analyses of diffraction intensities indicate that (i) the texture structure causes a monotonic reduction of peak intensity with increase of scattering vector including fundamental reflection and (ii) that layer thickness fluctuations in the range of one or two monolayers cause peak broadening and intensity reduction only for the higher-order satellite reflections. Observed satellite intensities could be reproduced by a model calculation which takes into consideration these two effects.

1. Introduction

Epitaxial superlattice films have been prepared for various combinations of metals [1]. Most of them are those where the two constituents have the same crystal structure and nearly equal lattice parameters. Recently, the authors have investigated multilayered films composed of Mn and Sb with different crystal structures [2–4]. Epitaxial superlattice films are obtained when Mn layers one or two monolayers thick are sandwiched by Sb layers 50 Å thick. The magnetic properties of Mn/Sb superlattice films are interesting. They are ferromagnetic, although Mn metal is antiferromagnetic and Sb metal is non-magnetic. The ferromagnetism originates from intermetallic compound MnSb [5] formed by interfacial reaction. Deposited Mn layers are so thin that all Mn atoms react to form epitaxial MnSb/Sb multilayered films. As was already reported, a sample containing MnSb one monolayer thick shows a ferromagnetism with perpendicular magnetic anisotropy [2]. Also it was found that the magnetic anisotropy is strongly dependent on MnSb layer thickness [3]. These magnetic properties should closely relate with the structural properties of very thin MnSb layers.

Structural characterizations are crucial for the investigation of metallic multilayered films with artificial superstructures. X-ray diffraction is one of the most basic and non-destructive methods to find the average structures and degree of structural perfection [6, 7]. In this paper, results of x-ray diffraction study for several Mn/Sb multilayered films are presented. In particular, structures of MnSb/Sb superlattice films containing MnSb one or two monolayers thick have been studied in detail. Modulation wavelength,

0953-8984/90/499717 + 17 $03.50

texture and coherency strain have been investigated following the normal procedures [6, 8]. Also diffraction intensities have been analysed based on a simple model called the step model [6, 7]. The effects of the one-dimensional disorder on the x-ray diffraction profiles of metallic multilayered films have been investigated by many researchers [7, 9–11]. The present MnSb/Sb multilayered films have also shown experimental results that indicate some structural imperfections. In this paper, effects of fibre texture structure and fluctuation in the number of atomic planes will be discussed. The former have never been taken into consideration in previous diffraction intensity analyses. Electron microscopy is also a powerful tool for the structural characterization, especially on the local structures, although it is a destructive method. The results of electron microscopy on a sample containing monolayer-thick MnSb have been published elsewhere [4]. They revealed the formation of a coherent multilayered structure. Magnetic properties of ferromagnetic MnSb monolayers and submonolayers will be reported in a forthcoming paper [12].

2. Structural aspect of Mn/Sb multilayered films

Antimony crystallizes into As-type (A7) structure ($R\bar{3}m$) and the lattice parameters are $a = 4.308$ Å and $c = 11.273$ Å in a hexagonal system [13]. The crystal structure of Sb is layered. The unit layer (zigzag net plane) consists of two triangular lattice planes, whose separation is 1.51 Å. The spacing between unit layers is 3.76 Å ($= d(003)$). Unit layers are stacked along the c axis in a FCC mode. Thin films of Sb grow with [00.1] orientation under appropriate deposition conditions [14, 15]. Unit layers of Sb are stacked along the growth direction in thin films.

Manganese metal has a complex crystal structure (α-Mn type, $I\bar{4}3m$, $a = 8.892$ Å) at room temperature [16]. When thin manganese films are deposited on Sb films, Mn atoms react with Sb atoms to form the intermetallic compound MnSb at the interfaces. The interfacial reaction occurs even when the substrate temperature is kept at room temperature. A Mn layer 40 Å thick in a Sb(300 Å)/Mn(40 Å)/Sb(100 Å) sandwiched film has been found to turn to a MnSb film 143 Å thick epitaxially grown between Sb layers [4]. The non-stoichiometric intermetallic compound $Mn_{1+x}Sb$ has a NiAs-type structure ($P6_3/mmc$) with lattice dimensions of $a = 4.128$ Å and $c = 5.787$ Å for $x = 0.02$ [17]. Lattice parameters of the 143 Å thick epitaxial MnSb layer are close to those of nearly stoichiometric MnSb [4]. The orientational relationship of the epitaxy was found to be $(00.1)_{Sb}\|(00.1)_{MnSb}$; $[11.0]_{Sb}\|[11.0]_{MnSb}$ in the previous x-ray diffraction and electron microscopy study [4]. Also, in the superlattice films, Sb and MnSb layers are stacked keeping the orientational relationships described above. Lattice matching of MnSb with Sb is fairly good, because in both Sb and MnSb lattices Sb triangular lattice planes are stacked along the c axis, in a HCP mode in MnSb and in a FCC mode in Sb. The in-plane lattice misfit $(a_{MnSb} - a_{Sb})/a_{Sb}$ is -4.5%.

3. Experimental details

Samples were prepared by an alternate vapour deposition method in an ultrahigh vacuum system. The pressure before the deposition was about 10^{-9} Torr. Layer thicknesses and deposition rates were measured during deposition by a quartz oscillator thickness monitor; a typical deposition rate was 0.2 Å s^{-1}. The substrates were glass plates and polyimide films. The substrate temperature was kept at room temperature

Table 1. List of samples and their deposition conditions. The thicknesses of each layer are nominal ones. A buffer Sb layer was deposited and then multilayered films were deposited. Sample E is a 1000 Å thick Sb film. Superlattice periods Λ were determined by x-ray diffraction.

Sample	D_{Mn} Mn layer thickness (Å)	D_{Sb} Sb layer thickness (Å)	Number of bilayers	Thickness of buffer Sb layer (Å)	Substrate temperature (°C)	Period Λ (Å)
A	12	120	28	600	22	
B	4	50	70	1000	23	60.7
C	2	50	90	1000	33	55.6
D	1	50	90	700	22	51.2
E	—	—	—	1000	30	

during deposition. A thick Sb buffer layer was deposited before the alternate deposition of Mn and Sb. Buffer layers of Sb have a [00.1] texture of hexagonal A7-type structure. However, in-plane orientations are at random. Although crystalline substrates (such as Al_2O_3, NaCl and GaSb) were examined, Sb layers deposited on these substrates had poorer crystallinity than those deposited on glass or polyimide films. For magnetic measurements, we have used samples deposited on 7.5 μm thick polyimide films. Most of the results described in this paper are for samples deposited on polyimide films. No distinct difference was found between samples deposited on glass and polyimide. Deposition conditions and nominal individual Mn and Sb layer thicknesses (D_{Mn} and D_{Sb}) of prepared samples are listed in table 1. The Sb layer thicknesses in the multilayers were always thicker than 50 Å, because the thinner Sb layers caused poor crystallinities of multilayered films.

X-ray diffraction patterns were measured by a computer-controlled four-circle diffractometer (Huber 420/511.1). Cu–Kα radiation (λ = 1.54184 Å) from a rotating-anode-type source (Rigaku RU-300) was used. Incident x-rays were monochromatized by a flat pyrolytic graphite (PG) 00.2 crystal. Another flat PG 00.2 crystal was placed in the diffracted beam path as an analyser. The present multilayered films have fibrous texture structures and cylindrical symmetry. Hereafter, the z and x axes in real space denote the growth direction (fibre axis, perpendicular to the film) and the equatorial direction (parallel to the film), respectively. The corresponding reciprocal axes are denoted as the $Q_\perp$ and $Q_\parallel$ axes, respectively. The following scanning modes of the diffractometer were employed:

(i) $Q_\perp$ axial scan mode: θ–2θ radial scan with the scattering vector Q perpendicular to the film plane ($Q_\parallel = 0$; symmetrically reflecting condition).

(ii) $Q_\parallel$ axial scan mode: θ–2θ radial scan with Q parallel to the film plane ($Q_\perp = 0$; transmitting condition).

(iii) Rocking scan mode: ω scan, fixing the counter position 2θ.

(iv) $Q_\perp$ off-axial scan mode: ω, 2θ independent scan along an arbitrary line parallel to $Q_\parallel = 0$ in reciprocal space.

(v) $Q_\parallel$ off-axial scan mode: ω, 2θ independent scan along an arbitrary line parallel to $Q_\perp = 0$.

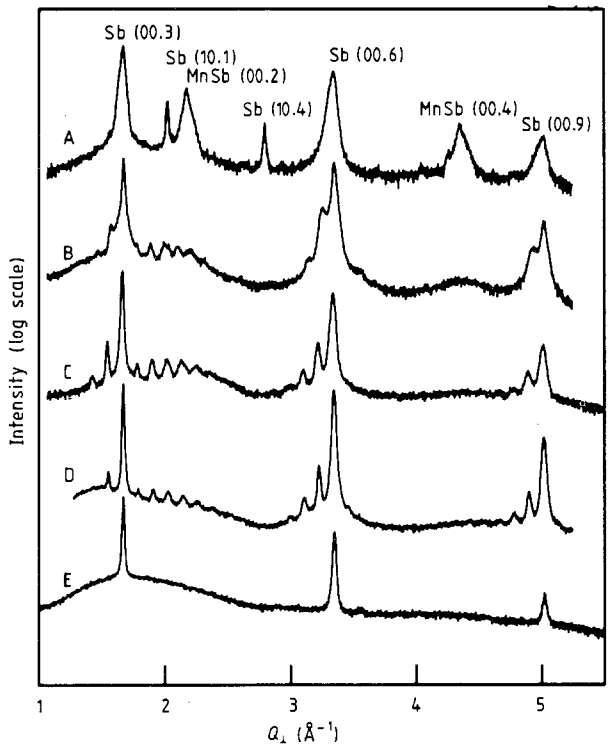

Figure 1. X-ray diffraction profiles in the $Q_\perp$ axial scan mode for samples A to E. The ordinate shows intensities in a logarithmic scale. All samples show strong peaks at around Sb(00.3m) reflections, indicating [00.1] orientations of Sb layers. Sample A shows (00.2) and (00.4) reflections of MnSb formed by the interfacial reaction. Satellite peaks are seen in the diffraction pattern of samples B, C and D. Substrates of samples A, B, C and D are polyimide films and that of sample E is a glass plate. The very broad peaks at around Q = 1.5–2.0 Å^{-1} are those from substrates with amorphous structures.

The instrumental resolution in the radial θ–2θ scan modes measurd using a Ge 111 perfect crystal was 0.010 ± 0.001 Å^{-1} in Q ($= 4\pi \sin\theta/\lambda$).

4. Results and discussion

4.1. Layer stacking and texture structure

Figure 1 shows x-ray diffraction patterns observed in the $Q_\perp$ axial scan mode for the samples listed in table 1. All diffraction patterns show sharp peaks at around (00.3m) (m = integer) reflections of Sb metal. Other peaks of Sb are too weak to be observed except for the case of sample A. Antimony layers in these multilayered structures have the [00.1] orientation of hexagonal A7-type structure as well as the Sb buffer layer. Sample A (D_{Mn} = 12 Å) shows broad (00.2) and (00.4) reflections of intermetallic compound MnSb. Neither peaks of Mn metal nor other peaks of MnSb were observed. Therefore, all the Mn atoms have reacted with Sb to form [00.1]-oriented MnSb layers. However, no superlattice peak was detected. The interfaces in sample A are rather rough.

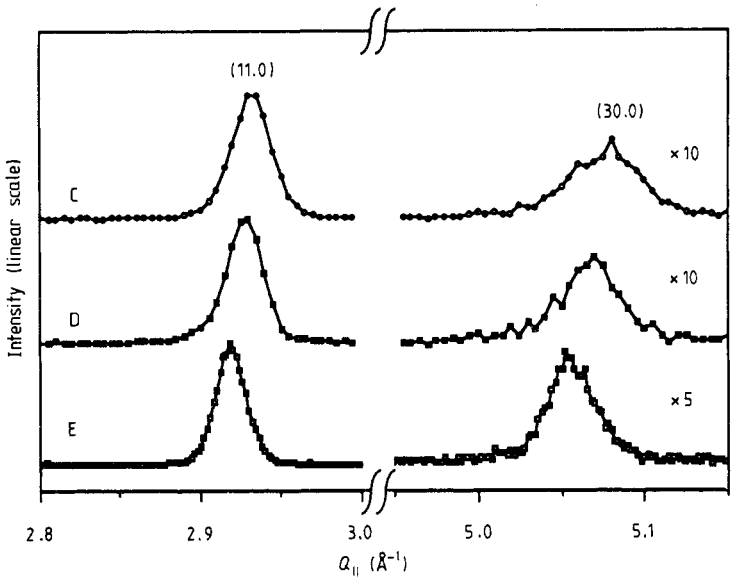

Figure 2. X-ray diffraction profiles observed in the $Q_{\parallel}$ axial scan mode for samples C, D and E. Both Sb (11.0) and (30.0) peaks appear in one scan even in the case of sample E.

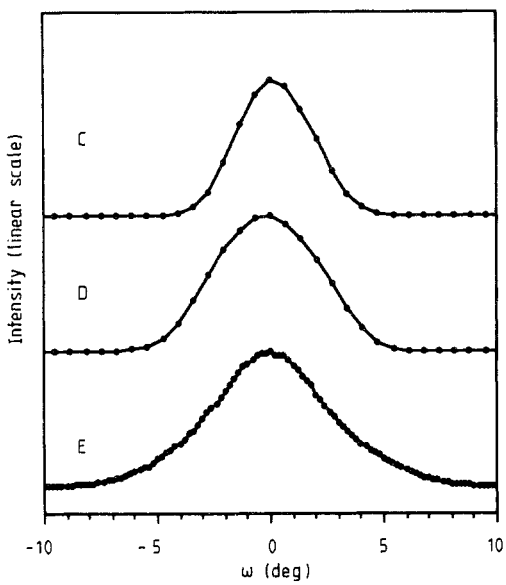

Figure 3. Rocking curves of $(00.3)_0$ fundamental reflections for samples C, D and E.

Diffraction patterns of sample B (D_{Mn} = 4 Å), C (D_{Mn} = 2 Å) and D (D_{Mn} = 1 Å) show many satellite peaks which indicate coherent stacking of MnSb and Sb layers. Also in the small-Q range, the first-order superlattice peaks were detected for samples deposited on glass plates. Hereafter, fundamental reflections referring to Sb lattice are denoted as $(00.3m)_0$ and their satellite peaks as $(00.3m)_n$, where positive values of n

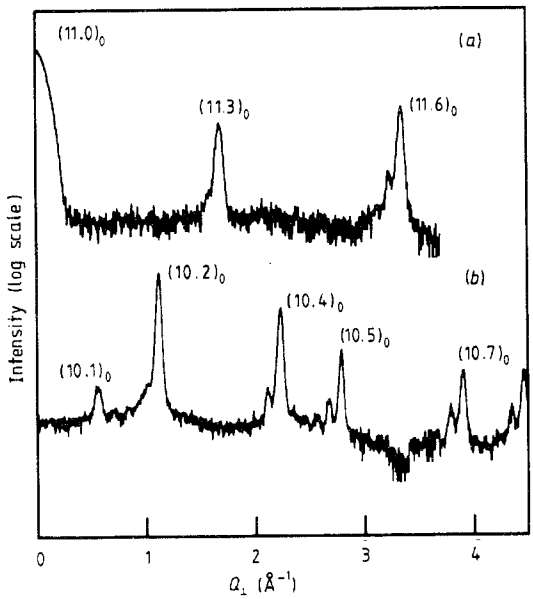

Figure 4. X-ray diffraction profiles of sample C in the $Q_\perp$ off-axial scan modes to trace (*a*) [11.L]* and (*b*) [10.L]* reciprocal rows of Sb lattice. Several satellites are seen and are indicative of good structural coherence.

mean satellite peaks on the high-Q side. From the satellite spacings, superlattice periods were determined. They are listed in table 1. The periods determined by x-ray diffraction are slightly larger than nominal ones ($D_{Mn} + D_{Sb}$) measured by a quartz oscillator thickness monitor during deposition. Because both fundamental and satellite peaks are as sharp as peaks of Sb thin film of 1000 Å thickness (sample E), coherent lengths along the growth direction are fairly long in these samples. Also, it is reasonable to assume that MnSb layers have the same crystallographic orientations as those in much thicker MnSb layers sandwiched by Sb layers.

Sharp satellite reflections of samples C and D indicate that epitaxial MnSb/Sb superlattice films are obtained. The film qualities of these samples have been investigated. Figure 2 shows diffraction patterns of samples C, D and E observed in the $Q_\parallel$ axial scan mode. In arbitrary setting of in-plane orientation of the sample, diffraction patterns show both Sb(11.0) and Sb(30.0) reflections. The absence of other reflections is evidence of the [00.1] orientation of Sb layers. The appearance of both reflections, however, indicates random orientations in the film plane. Thus films have fibre texture structures. The fibre texture structures of superlattice films are inevitable because Sb buffer layers have fibre texture structures. Peak widths of (11.0) reflection for multilayered films are nearly equal to that for Sb buffer layer (sample E). An electron microscopy observation has indicated that the in-plane grain size of Sb buffer layer is about 2000 Å and that each grain gives a single crystalline electron diffraction pattern. However, crystallographic coherence lengths in the film plane calculated from the FWHM (full width at half maximum) of Sb(11.0) peaks are about 300 Å for samples C, D and E. A smaller coherence length may be due to defects in the films.

Figure 3 shows rocking curves of $(00.3)_0$ fundamental reflections for samples C, D and E. Their FWHMs are about 10° in ω, which indicate a distribution in growth orientation. No distinct difference was observed between the Sb buffer layer (sample E) and superlattice films (samples D and C). Satellite reflections have nearly equal FWHMs of the rocking

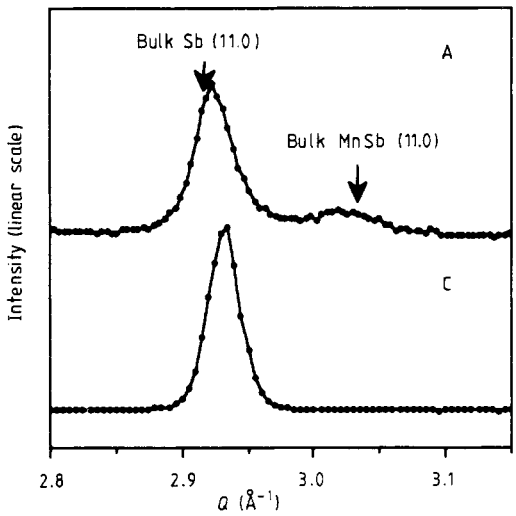

Figure 5. A comparison of peak positions of Sb(11.0) reflection for samples A and C. Sample A shows both Sb(11.0) and MnSb(11.0) peaks. The $(11.0)_{Sb}$ lattice spacing is almost the same as that in bulk Sb metal. However, the Sb(11.0) peak of sample C has shifted to higher Q, which indicates the contraction of Sb lattice in the film plane.

curve to those of fundamental reflections. The distribution of growth orientation in the superlattice films is nearly the same as that of Sb buffer layers.

Although the films have fibre texture structures, the crystallographic coherence between adjacent 50 Å thick Sb layers is fairly good across the MnSb layers in each grain. Figure 4 shows diffraction patterns of sample C observed in the $Q_\perp$ off-axial scan mode to trace [11.L]* and [10.L]* reciprocal rows with respect to the Sb lattice. They show fundamental reflections, $(10.1)_0$, $(10.2)_0$, $(10.4)_0$ and $(10.5)_0$ in [10.L]* row and $(11.0)_0$, $(11.3)_0$ and $(11.6)_0$ in [11.L]* row, accompanied by satellite peaks. The satellite peaks give clear evidence of structural coherence along [10.1] or [10.2] etc as well as along the growth direction [00.1]. The absence of $(10.0)_0$, $(10.3)_0$ and $(10.6)_0$ fundamental reflections in the [10.L]* row is because of the rhombohedral symmetry of Sb lattice. The appearance of both $(10.1)_0$ and $(10.2)_0$ peaks in a [10.L]* row is because of the texture structure.

Both Sb and MnSb layers in the MnSb/Sb superlattice films are strained because of an in-plane lattice misfit of about -4.5%. Figure 5 shows peak profiles of samples A and C at around Sb(11.0) reflection observed in the $Q_\parallel$ axial scan mode. The thicknesses of individual MnSb layers calculated from the nominal Mn thicknesses D_{Mn} are 43 and 7 Å for samples A and C, respectively. The diffraction pattern of sample A shows both Sb(11.0) and MnSb(11.0) reflections. Lattice spacings are $d(11.0)_{Sb} = 2.15$ Å and $d(11.0)_{MnSb} = 2.08$ Å. The observed $d(11.0)_{Sb}$ is close to that of bulk Sb metal (2.154 Å) but $d(11.0)_{MnSb}$ is larger than bulk $d(11.0)_{MnSb}$ (2.064 Å). Thus 43 Å thick MnSb layers in sample A are strained. The diffraction pattern of sample C shows only an Sb(11.0) peak. It was shifted to a higher angle although the Sb(11.0) peak from buffer layer is overlapped. The peak position gives an Sb(11.0) lattice spacing of 2.143 Å, which is 0.5% smaller than lattice spacing (2.154 Å) in bulk Sb metal or sample A. The highly coherent structure of sample C has caused lattice strains in 50 Å thick Sb layers. Because 43 Å thick MnSb layers in sample A are strained, the absence of MnSb(11.0) peak in the diffraction pattern of sample C indicates that 7 Å thick MnSb layers in sample C have the same in-plane lattice spacings as those in Sb layers. The diffraction pattern of

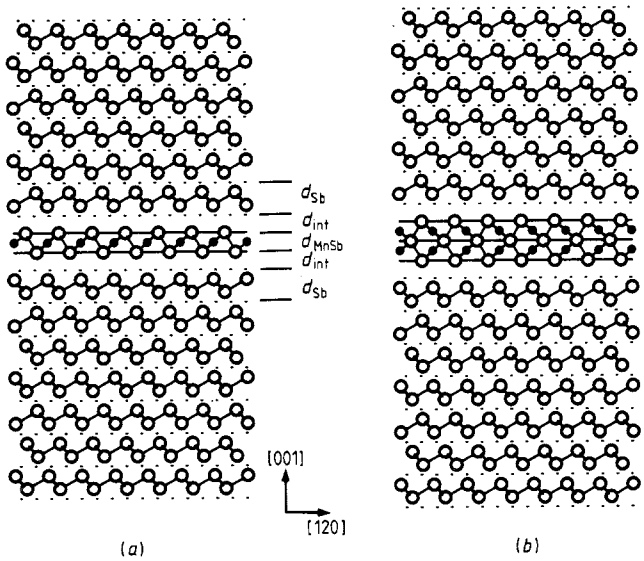

Figure 6. Model structures of MnSb/Sb superlattice films based on the step model viewed along [10.0] direction of Sb lattice: ○, Sb; ●, Mn. (*a*) A unit cell with 1 monolayer (ML) thick MnSb. (*b*) A unit cell with 2 ML thick MnSb. Both Sb and MnSb layers are stacked keeping epitaxial orientations $(00.1)_{MnSb}\|(00.1)_{Sb}$; $[11.0]_{MnSb}\|[11.0]_{Sb}$. In both structures, the number of Sb layer units (zigzag net planes) is 13 and their spacings d_{Sb} are always equal to 3.76 Å ($=d(00.3)_{Sb}$). In the intensity calculation, the lattice spacing in MnSb layers, d_{MnSb}, and the lattice spacing at the interface, d_{int}, were varied.

sample D also shows a similar peak shift of Sb(11.0) reflection to that seen in figure 4. Thus, what is called strained layer superlattices [18] are obtained for samples C and D.

4.2. Structure model and intensity analysis

To elucidate atomic arrangements in the epitaxial superlattice films (samples C and D), x-ray diffraction profiles have been calculated based on several model structures and they have been compared with observed diffraction patterns in the $Q_\perp$ axial scan mode.

4.2.1. Step model. At first, observed intensities are compared with calculated ones for ideal model structures based on the 'step model' [6, 7], often used in the intensity analyses for metallic multilayered films. The step model assumes that the lattice spacings in the individual layers are constant. Model structures for samples D and C viewed along [10.0] direction of the Sb layer are shown in figure 6(*a*) and (*b*), respectively. According to the orientational relationship of epitaxy between MnSb and Sb layers, $(00.1)_{Sb}\|(00.1)_{MnSb}$; $[110]_{Sb}\|[110]_{MnSb}$, Sb unit layers (zigzag net plane) and MnSb unit layers are stacked along their *c* axes. The thickness of a Sb layer unit d_{Sb} is equal to $d(00.3)_{Sb}$. One MnSb layer unit means a lattice slab with the thickness d_{MnSb} equal to a half of the unit dimension *c* of NiAs-type structure. It contains one Mn lattice plane and is to be denoted as MnSb 1ML (monolayer). If the numbers of unit layers are N_{Sb} and N_{MnSb} in a unit period Λ, positions of lattice planes along the stacking direction are given by the following equation:

(i) For Sb lattice planes in the Sb layer

$$(j+z_{Sb})d_{Sb} \qquad (j=0,1,\ldots,N_{Sb}-1)$$

$$(j-z_{Sb})d_{Sb} \qquad (j=1,2,\ldots,N_{Sb}).$$

(ii) For Sb lattice planes in the MnSb layer

$$jd_{MnSb}+N_{Sb}d_{Sb}+d_{int} \qquad (j=0,1,\ldots,N_{MnSb}).$$

(iii) For Mn lattice planes

$$(j+\tfrac{1}{2})d_{MnSb}+N_{Sb}d_{Sb}+d_{int} \qquad (j=1,2,\ldots,N_{MnSb})$$

$$\Lambda = N_{Sb}d_{Sb}+N_{MnSb}d_{MnSb}+2d_{int}.$$

In the above equations, z_{Sb} denotes a positional parameter of Sb lattice planes in a Sb unit layer and d_{int} denotes the 'interface spreading'. The Sb–Sb lattice spacing at the interface is given by $d_{int}+z_{Sb}d_{Sb}$.

In the intensity calculations, the structures of Sb layers are assumed to be the same as for bulk Sb metal, namely $d_{Sb}=3.76$ Å and $z_{Sb}=0.301$. The numbers of unit layers were fixed to be $N_{Sb}=13$ for both samples D and C, $N_{MnSb}=1$ for sample D and $N_{MnSb}=2$ for sample C, so that unit periods and individual layer thicknesses nearly agree with the observed periods and nominal thicknesses D_{Mn} and D_{Sb}. Diffraction profiles were calculated by varying only two parameters, d_{MnSb} and d_{int}. The in-plane lattice dimensions of the MnSb and Sb layers are equal. The calculation takes the Lorentz polarization factor into account but not absorption or thermal factors. A Gaussian profile function with a width of 0.010 $Å^{-1}$ (instrumental resolution) was convoluted with the calculated profiles.

Figure 7(*a*) shows a calculated diffraction profile of the model structure for sample D ($D_{Mn}=1$ Å) in figure 6(*a*). Values of parameters are $d_{int}=0.35$ Å and $d_{MnSb}=2.80$ Å. For comparison, the observed profile is also shown in the figure. The calculation could reproduce qualitative features of observed profile; the $(00.3m)_{-1}$ peaks are much more intense than $(00.3m)_{+1}$ peaks and $(00.3)_{+n}$ satellite peaks near the bulk MnSb(00.2) reflection are fairly intense. The interference of x-rays diffracted by Sb lattice planes in the adjacent Sb layers mainly contributes to satellite reflections with small $|n|$. In other words, the thickness of MnSb layers or $d_{MnSb}+2d_{int}$ determines the satellite intensities with small $|n|$. A variation of about 0.1 Å in $d_{MnSb}+2d_{int}$ causes a distinct deviation from observed intensity ratios, particularly for $(00.9)_{\pm 1}$ satellite reflections. Therefore, the probable errors of parameters are less than ±0.1 Å. The ratio of d_{MnSb}/d_{int}, namely the structure of the MnSb layer, determines the relative intensities of satellite peaks at around the bulk MnSb(00.2) reflection.

Figure 7(*b*) shows a calculated diffraction profile of a model structure for sample C ($D_{Mn}=2$ Å) shown in figure 6(*b*). Values of parameters used in the calculation are $d_{int}=0.73$ Å and $d_{MnSb}=2.86$ Å. The observed profile is also supplemented for comparison. The qualitative features of satellite intensities are reproduced as well as the case of sample D. The values of d_{MnSb} for samples C and D are nearly equal to $d(00.2)_{MnSb}=2.864$ Å of bulk MnSb. The values of d_{int} and d_{MnSb} for sample D are smaller than those for sample C. They may be indicative of the lattice strain in MnSb monolayers along the *c* axis. Further quantitative arguments, however, are not possible, because values are average ones for superlattices with layer thickness fluctuation, as will be mentioned in section 4.2.3.

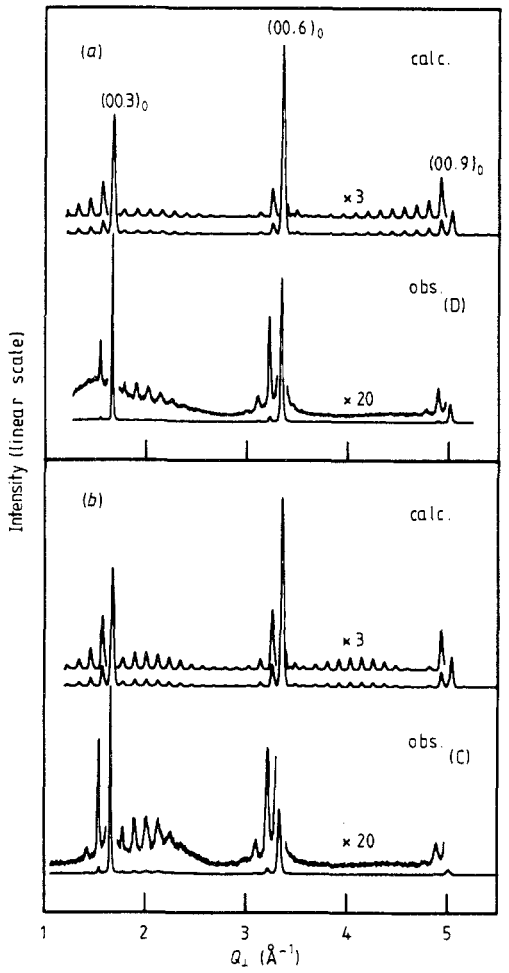

Figure 7. Calculated diffraction profiles in $Q_\perp$ axial scan mode for the two model structures in figure 6(*a*) and (*b*). Ordinates show intensities in linear scale. For comparison, observed profiles of samples D and C are also shown. The values of parameters in the model structures are (*a*) $d_{MnSb} = 2.08$ Å, $d_{Sb} = 3.76$ Å and $d_{int} = 0.35$ Å, (*b*) $d_{MnSb} = 2.86$ Å, $d_{Sb} = 3.76$ Å and $d_{int} = 0.73$ Å. The two plots in each figure show the same data with different magnifications.

The calculated diffraction profiles in figure 7(*a*) and (*b*) based on the step model reproduce typical features of the observed diffraction patterns. However, between calculated and observed diffraction patterns there are two outstanding discrepancies.

The first is that $(00.6)_0$ fundamental reflections are much stronger than $(00.3)_0$ fundamental reflection in the calculated diffraction patterns, although in the observed diffraction patterns $(006)_0$ peaks are weaker than $(003)_0$ peaks. The intensity ratio, $I(003)_{Sb}/I(006)_{Sb}$, is very similar to that in the diffraction pattern of 1000 Å thick Sb film (sample E). The Debye–Waller factor, which was not taken into consideration in the above calculations, may be one of the reasons. However, it could not explain the observed intensity ratios. Values of the Debye–Waller factor, $\exp\{-2B[(\sin\theta)/\lambda]^2\}$, were calculated using a thermal factor $B = 0.69$ Å^2 at room temperature for Sb metal reported in the literature [13]. They are 0.97 at (00.3) reflection and 0.91 at (00.6) reflection. To reproduce the observed intensity ratio, B should be a large value of about 13 Å^2.

The second discrepancy is that in the calculated diffraction patterns, the satellite peaks between $(00.6)_0$ and $(00.9)_0$ fundamental reflections have fairly large intensities, especially near the MnSb(00.4) reflection. However, observed diffraction patterns show no peaks near MnSb(00.4) reflections.

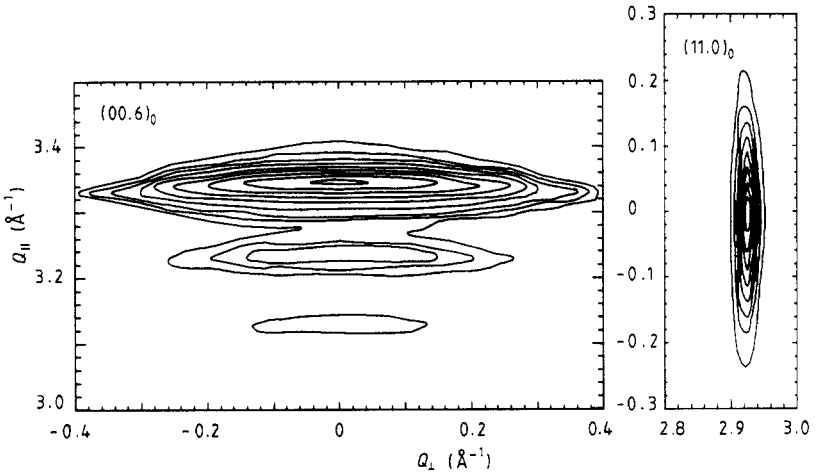

Figure 8. Contour maps of x-ray diffraction intensities of $(00.6)_0$ and $(11.0)_0$ fundamental reflections for sample D derived from several measurements in the $Q_\perp$ and $Q_\parallel$ off-axial scan modes. Contour intervals are one-tenth of peak values. Note that the intensity distribution for $(00.6)_0$ reflection is elongated along the $Q_\parallel$ axis but that intensity distribution for Sb (11.0) reflection is elongated along the $Q_\perp$ axis. The mosaic spread is a main contribution of peak broadening.

The first discrepancy is caused by the texture structure and the second is caused by the fluctuation of superlattice period, as will be discussed below.

4.2.2. Effect of fibre texture on the diffraction pattern. As mentioned in section 4.1, samples C and D have fibre texture structures. The films consist of small crystallites in which the c axes of both Sb and MnSb layers are aligned nearly along the growth direction z. Azimuthal orientations of crystallites in the film plane are at random. A typical feature of x-ray diffraction patterns for fibre texture structure is the broadening of diffraction peaks caused by both small particle size and the distribution of particle orientations. For example, contour maps of intensity near $(00.6)_0$ peak on the fibre axis and $(11.0)_0$ peaks on the equatorial axis for sample D are shown in figure 8. Observed intensity distribution of the $(00.6)_0$ peak shows an elongation along the $Q_\parallel$ axis whereas that of $(11.0)_0$ is along the $Q_\perp$ axis. This means that the distribution of particle orientations has a dominant role in the peak broadening.

The effects of grain orientation distribution (mosaic spread) on diffraction profiles have been studied for the crystalline polymers which also have fibre texture structures [19]. In the light of a recent review by Fraser and co-workers [20], the effects of the texture structure on the diffraction patterns of samples C and D will be discussed in this section.

We have assumed an orientational distribution function of crystallites $G(\alpha)$ with a Gaussian shape:

$$G(\alpha) = \frac{2}{\alpha_0^2} \exp\left(-\frac{\alpha^2}{2\alpha_0^2}\right) \tag{1}$$

where α and α_0 are a departure angle of the c axis of a particle from the fibre axis and its standard deviation, respectively. No distribution of particle sizes was assumed. In the

following, P_z and P_x denote average particle dimensions along the z axis (fibre axis or growth direction) and x axis (in the film plane), respectively. The total diffraction intensities from an assembly of crystallites, $I_s(Q_\perp, Q_\parallel)$, are given by the integration of intensities from individual particles, $I_p(Q_\perp, Q_\parallel)$. In a spherical polar coordinate system, $I_s(Q_\perp, Q_\parallel)$ is expressed by

$$I_s(Q, \sigma_s) = \frac{1}{\alpha_0^2} \int I_p(Q, \sigma_p) \exp\left[\frac{-(\sigma_p - \sigma_s)^2}{2\alpha_0^2}\right] i_0\left[\frac{\sin\sigma_s \sin\sigma_p}{\alpha_0^2}\right] \sin\sigma_p \, d\sigma_p \tag{2}$$

$$i_0(x) = \exp(x) I_0(x)$$

$$Q = \sqrt{Q_\parallel^2 + Q_\perp^2}$$

$$\sigma = \tan^{-1}(Q_\parallel / Q_\perp)$$

where $I_0(x)$ is the modified Bessel function of the second kind of order zero.

This equation gives the approximate peak widths of reflections at specific positions as follows: for reflections on the fibre axis ($Q_\parallel = 0$):

width along $Q_\perp$ axis $\quad \Delta Q_\perp = 2\sqrt{(\log 2/\pi)}/P_z$

width of rocking curve $\quad \Delta\omega_\perp = 2\sqrt{[\log 2/\pi(2\pi\alpha_0^2 + 4\pi^2/Q_\perp^2 P_x^2)]}$

and for those on the equatorial axis ($Q_\perp = 0$):

width along $Q_\parallel$ axis $\quad \Delta Q_\parallel = 2\sqrt{(\log 2/\pi)}/P_x$

width of rocking curve $\quad \Delta\omega_\parallel = 2\sqrt{[\log 2/\pi(2\pi\alpha_0^2 + 4\pi^2/Q_\parallel^2 P_z^2)]}$.

Observed peak widths are $\Delta Q_\perp = 0.013$ Å^{-1}, $\Delta\omega_\perp = 10°$ for $(00.3)_0$ reflection and $\Delta Q_\parallel = 0.026$ Å^{-1}, $\Delta\omega_\parallel = 10°$ for Sb(11.0) reflection, respectively. From these values and the above equations, average particle dimensions and standard deviations of particle orientation were determined to be $P_x = 300$ Å, $P_z = 500$ Å and $\alpha_0 = 5°$. It is to be noted that values of P_x and P_z are crystallographic coherence lengths. They are strongly affected by lattice distortions and lattice defects.

As for the peak intensities on the fibre axis, equation (2) is approximated by

$$I(Q, 0) = I_p(Q, 0) \frac{1}{1 + Q^2 P_x^2 \alpha_0^2}. \tag{3}$$

This equation means that the fibre texture structure reduces the peak intensities of higher-order reflections by a factor of $1/(1 + Q^2 P_x^2 \alpha_0^2)$ with a Lorentzian form. Hereafter, this factor is denoted as 'texture factor'. For sample D, the observed peak intensity ratio, $I(00.3)_0/I(00.6)_0$, is 2.9 whereas the calculated one shown in figure 7(*a*) is 0.62. The values of 'texture factor' derived from the observed value of P_x and α_0 are 1.9×10^{-4} at the $(00.3)_0$ peak and 4.7×10^{-5} at $(00.6)_0$ peak, respectively. Multiplying these values on the calculated profile in figure 7(*a*), intensity ratio $I(00.3)_0/I(00.6)_0$ becomes 2.5 which agrees with the observed one. Thus the relative intensities of fundamental reflections could be reproduced by taking the effect of texture structure into account.

4.2.3. Layer thickness fluctuation. The 'texture factor' in equation (3) is one of the origins of the observed weak intensities of satellite reflections at around the (00.4) reflection of bulk MnSb. However, it is not enough to explain the observed intensities. Another factor to be taken into account is the layer thickness fluctuation. In the present sample

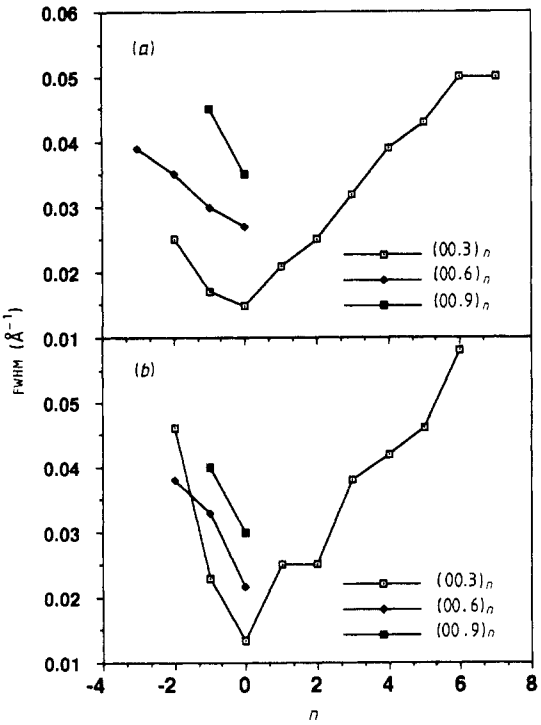

Figure 9. Observed peak width of satellite reflection $(00.3m)_n$ plotted as functions of n for (*a*) sample D and (*b*) sample C. Satellite peaks increase their width with increasing $|n|$. Such a peak broadening is indicative of the random mixture of different supercell periodicities.

preparation conditions, it is difficult to control the individual layer thicknesses with an accuracy less than 1 Å; some fluctuation in layer thickness may exist.

An effect of layer thickness fluctuation clearly appears in the observed line widths of the satellite reflections. Figure 9 shows observed peak widths for samples C and D. The peak width of satellite reflection $(00.3m)_n$ increases with increasing $|n|$, although fundamental reflections $(00.3m)_0$ do not show such large line broadening with increasing m. The increase for fundamental reflections is ascribable partly to lattice strain or defects in Sb layers, because a similar line broadening was also observed for a 1000 Å thick Sb film (sample E). The line broadening of higher-order peaks for metallic superlattice films is evidence of fluctuation in the layer thickness or modulation wavelength. Similar results have been reported for Gd/Y superlattice films [7].

The problem of one-dimensional disorder in the multilayered structure has been discussed by many researchers. Fujii and co-workers [9] and more recently Locquet and co-workers [10] have described the effect of disorder, mainly concentrated at the interfaces, for crystalline/crystalline superlattices. They have assumed a continuous Gaussian fluctuation of superlattice period. In this case, the peak width increases monotonically with Q or reflection order. This is not the case for the present Mn/Sb superlattice films. On the other hand, Clemens and Gay [11] have discussed the case with discrete fluctuation in the number of atomic planes. They have pointed out that fluctuations in the range of 1 or 2 Å does not cause the line broadening of high-angle peaks and only causes a reduction of peak intensity for satellite reflections. This also is not the case. Besides multilayered films, the peak broadening of superlattice reflections has been studied for one-dimensionally disordered crystals like layered minerals [21] or

graphite intercalation compounds [22]. It has been shown that a random and homogeneous mixture of different superlattice periods, namely a discrete disorder, is the origin of peak broadening. Using a formula of Kakinoki and Komura [23], the effect of layer thickness fluctuation was simulated.

In the case of sample D, the average thickness of MnSb strictly calculated from the nominal thickness of Mn (D_{Mn}) is 1.2 MLs (monolayers). For simplicity, we have assumed that the number of Sb lattice planes in each Sb layer is constant ($N_{Sb} \equiv 13$) and that the number of Mn lattice planes in MnSb layer is one or two. In other words, a random stacking of only two superlattice units, shown in figure 6(a) and (b), was assumed. The crystallographic parameters of these two units are the same as those used for calculating diffraction patterns in figure 7(a) and (b). For a random stacking of several layer units differing in their structure factors and thicknesses, the scattering intensity is given by the following equations when the kth kind of layer has a structure factor of F_k, a probability of being found (frequency) of P_k and a unit period of Λ_k [23]:

$$I_0(Q) = N\overline{|F|^2} + 2\,\mathrm{Re}\left(\sum_{m=1}^{N-1}(N-m)AT^{m-1}B\right) \tag{4}$$

$$\overline{|F|^2} = \sum_k P_k|F_k|^2 \qquad A = \sum_k P_k F_k \exp(\mathrm{i}\Lambda_k Q)$$

$$T = \sum_k P_k \exp(\mathrm{i}\Lambda_k Q) \qquad B = \sum_k F_k^*$$

where Re and * indicate the real part and the complex conjugate, respectively. The parameter N represents a coherence length in the number of unit layers. In the present case, suffixes $k = 1$ and 2 denote layer units containing one and two monolayers. For example, a calculated profile for $P_1 = 0.85$, $P_2 = 0.15$ and $N = 8$ is shown in figure 10(a). The Lorentz polarization factor and the 'texture factor' (3) were multiplied with $I_0(Q)$. The values of P_1 and P_2 correspond to an average layer thickness of 1.15 ML of MnSb. In the calculated profile, satellite reflections near the MnSb (00.4) reflection have been greatly reduced in intensity compared with that calculated by the step model (figure 7(a)), although fundamental reflections have not. Also the peak widths of satellite reflections $(00.3m)_n$ increase with increasing $|n|$ as shown in figure 11(a).

For the case of sample C with a nominal Mn layer thickness of 2 Å, diffraction profiles were simulated assuming random stackings of two kinds of layer unit containing 2 or 3 MLs of MnSb. The crystallographic parameters for the layer unit containing 2 MLs of MnSb ($k = 2$) are the same as those used in the above calculations. Those for the layer unit containing 3 MLs of MnSb ($k = 3$) are $d_{int} = 1.17$ Å, $d_{MnSb} = 2.88$ Å and $N_{Sb} = 13$. The calculated profile with $P_2 = 0.6$, $P_3 = 0.4$ and $N = 8$ is shown in figure 10(b). The values of P_2 and P_3 correspond to an average MnSb layer thickness of 2.4 MLs. The satellite peaks near MnSb(00.4) reflection are much smaller in their intensity than those calculated by the step model. Also satellite peaks show a line broadening with reflection order similar to the observed one (figure 11(b)).

As mentioned above, layer thickness fluctuation is an origin of weak satellite intensities at around MnSb(00.4) reflection. However, fully quantitative agreements were not obtained between observed and calculated profiles at the present stage. The frequency parameters P_k in the above calculations bear probable errors of more than ± 0.1. The layer thickness fluctuation of MnSb, however, seems to be in the thickness range between 1 and 2 ML. The layer thickness fluctuation in Sb layers was not taken into account in the above calculations. Also there may appear layer units with MnSb 3 MLs thick locally in

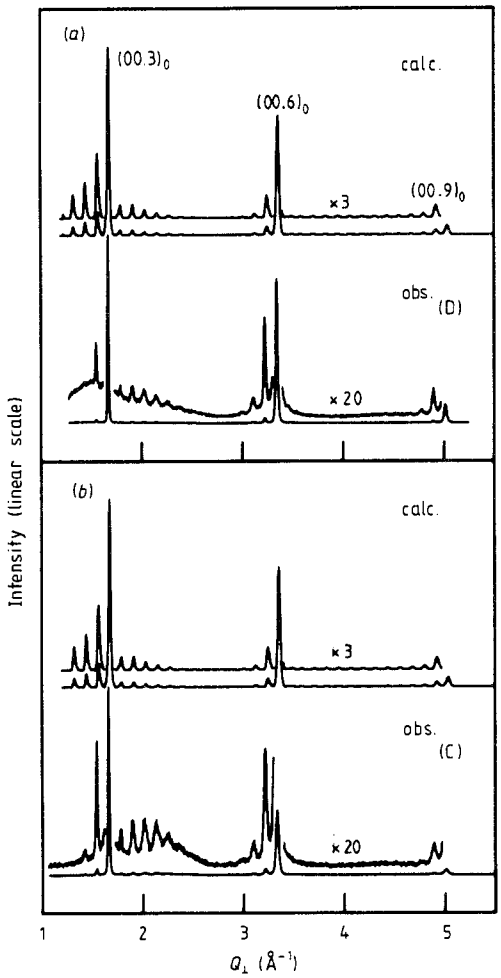

Figure 10. Calculated diffraction profiles in which the effects of both texture structure and mixed periodicity are taken into account. (*a*) A random mixture of two unit cells containing one and two MnSb monolayers. (*b*) A random mixture of two unit cells containing two and three MnSb monolayers. Note the differences from the profiles shown in figure 7 in the intensity of $(00.6)_0$ fundamental reflection and satellite reflections inbetween $(00.6)_0$ and $(00.9)_0$ fundamental reflections. See text for the details of calculation. The two plots for each figure show the same data with different magnifications.

sample D. In both cases, however, satellite peak intensities inbetween $(00.3)_0$ and $(00.6)_0$ fundamental reflections are greatly reduced, which does not agree with observations. It seems to be necessary for more quantitative agreements to take other factors into account, such as atomic steps in MnSb layers revealed by electron microscopy [4].

5. Conclusion

The results of the present x-ray diffraction investigation for Mn/Sb multilayered films are summarized as follows.

(1) MnSb/Sb superlattice films are obtained when nominal Mn layer thicknesses are 1 or 2 Å and Sb layer thicknesses are 50 Å.

(2) Superlattice films have fibre texture structures with in-plane grain size greater than 300 Å.

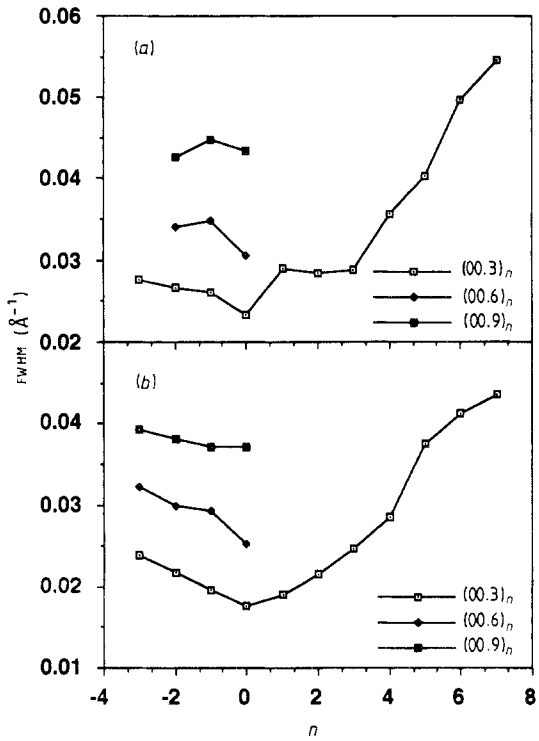

Figure 11. Peak widths in the calculated diffraction profiles shown in figures 10(*a*) and (*b*).

(3) Satellite intensities of superlattice films could be qualitatively reproduced by step model calculations assuming epitaxial orientations of $(00.1)_{MnSb}\|(00.1)_{Sb}$ and $[11.0]_{MnSb}\|[11.0]_{Sb}$.

(4) Texture structure reduces the diffraction intensities of high-Q reflections by a factor given by equation (3).

(5) An effect of layer thickness fluctuation was detected as peak broadening of satellite reflections. The higher-order reflection has a broader peak width although fundamental reflections do not show a large broadening with increase in the reflection order. Also, the layer thickness fluctuation causes a larger reduction of intensities for higher-order satellites, especially near the MnSb(00.4) reflection.

The degree of layer thickness fluctuation is very important to interpret magnetic properties of MnSb/Sb superlattice films, because the ferromagnetic transition temperatures and magnetic anisotropy of MnSb layers strongly depend on the thickness [3]. The present x-ray investigation and also magnetic measurements [12] suggest a layer thickness fluctuation in the range 1 or 2 monolayers of MnSb. Studies on the effect of layer thickness fluctuation of magnetic properties for samples including the present ones are in progress.

Acknowledgments

The authors are indebted to Mr H Dohnomae for his collaboration. This work was supported by a Grant-in-Aid for Scientific Research from the Ministry of Education, Culture and Science, Japan.

References

[1] Shinjo T and Takada T (eds) 1987 *Metallic Superlattice; Artificially Structured Materials* (Amsterdam: Elsevier)
[2] Shinjo T, Nakayama N, Moritani I and Endoh Y 1986 *J. Phys. Soc. Japan* **55** 2512
[3] Yamazaki H, Ajiro Y, Moritani I, Nakayama N and Shinjo T 1988 *J. Phys. Soc. Japan* **57** 4343
[4] Nakayama N, Moritani I, Shinjo T, Ishizaki A and Hajimoto K 1989 *Phil. Mag.* A **59** 547
[5] Okita T and Makino Y 1968 *J. Phys. Soc. Japan* **25** 120
[6] Fujii Y 1987 *Metallic Superlattice; Artificially Structured Materials* eds T Shinjo and T Takada (Amsterdam: Elsevier)
[7] McWhan D B 1989 *Physics, Fabrication and Application of Multilayered Structures* ed P Dhez and C Weisbuch (New York: Plenum) p 67
[8] Vook R W 1972 *Epitaxial Growth* ed J W Matthews (New York: Academic) p 339
[9] Fujii Y, Ohnishi T, Ishihara T, Yamada Y, Kawaguchi K, Nakayama N and Shinjo T 1986 *J. Phys. Soc. Japan* **55** 251
[10] Locquet J-P, Neerinck D, Stockman L, Bruynseraede Y and Schuller I K 1989 *Phys. Rev.* B **39** 13338
[11] Clemens B M and Gay J G 1987 *Phys. Rev.* B **35** 9337
[12] Moritani I, Nakayama N and Shinjo T 1990 *J. Magn. Magn. Mater.* **90–1**
[13] Barrett C S, Cucka P and Haefner K 1963 *Acta Crystallogr.* **16** 451
[14] Mojejko K, Paprpcki K, Subotowicz M and Radomsky M 1976 *J. Cryst. Growth* **36** 61
[15] Hashimoto M, Niizeki T and Kambe K 1980 *Japan. J. Appl. Phys.* **19** 21
[16] Gazzara C P, Middleton R M and Weiss R J 1967 *Acta Crystallogr.* **22** 859
[17] Nagasaki H, Wakabayashi I and Minomura S 1969 *J. Phys. Chem. Solids* **30** 329
[18] Osbourn G C 1984 *Thin Films and Interfaces II* ed J E E Baglin, C R Campbell and W K Chu (Amsterdam: North-Holland)
[19] Holmes K C and Leigh J B 1974 *Acta Crystallogr.* A **30** 635
[20] Fraser R D B, Suzuki E and MacRae T P 1984 *Structure of Crystalline Polymers* ed I H Hall (London: Elsevier) p 1
[21] Hendricks S and Teller E 1942 *J. Chem. Phys.* **10** 147
[22] Kim H J, Fischer J E, McWhan D B and Axe J D 1986 *Phys. Rev.* B **33** 1329
[23] Kakinoki J and Komura Y 1952 *J. Phys. Soc. Japan* **7** 30